Since January 2020 Elsevier has created a COVID-19 resource centre with free information in English and Mandarin on the novel coronavirus COVID-19. The COVID-19 resource centre is hosted on Elsevier Connect, the company's public news and information website.

Methods 54 (2011) 76–82

Contents lists available at ScienceDirect

Methods

journal homepage: www.elsevier.com/locate/ymeth

Applications of analytical ultracentrifugation to protein size-and-shape distribution and structure-and-function analyses

Chi-Yuan Chou *, Yi-Hui Hsieh, Gu-Gang Chang

Department of Life Sciences and Institute of Genome Sciences, National Yang-Ming University, Taipei 112, Taiwan

ARTICLE INFO

Article history:
Available online 16 November 2010

Keywords:
Analytical ultracentrifugation
Band-forming ultracentrifugation
Active enzyme centrifugation
Sedimentation velocity
Size-and-shape distribution
Quaternary structure

ABSTRACT

The rebirth of modern analytical ultracentrifugation (AUC) began in 1990s. Since then many advanced AUC detectors have been developed that provide a vast range of versatile choices when characterizing the physical and chemical features of macromolecules. In addition, there have been remarkable advances in software that allow the analysis of AUC data using more sophisticated models, including quaternary structures, conformational changes, and biomolecular interactions. Here we report the application of AUC to protein size-and-shape distribution analysis and structure-and-function analysis in the presence of ligands or lipids. Using band-sedimentation velocity, quaternary structural changes and an enzyme's catalytic activity can be observed simultaneously. This provides direct insights into the correlation between quaternary structure and catalytic activity of the enzyme. On the other hand, also in this study, we have applied size-and-shape distribution analysis to a lipid-binding protein in either an aqueous or lipid environment. The sedimentation velocity data for the protein with or without lipid were evaluated using the $c(s,f_r)$ two-dimensional distribution model, which provides a precise and quantitative means of analyzing the protein's conformational changes.

1. Introduction

Analytical ultracentrifugation (AUC)[1] is a very precise and powerful instrument for investigating the size distribution of macromolecules in solution. However, expensive instrumentation and laborious manual data handling somehow have resulted in this powerful instrument being ignored by most scientists. This situation has been changing since 1990s when computerized data acquisition becomes mature and was complemented by the launch of many sophisticated software packages that make the AUC data very informative. Furthermore, the development of various detectors, such as Schlieren optics, UV/VIS absorption, Rayleigh interference, fluorescence, light scattering, turbidity, and multiwavelength UV/VIS optics, has made AUC more versatile that never before [1–3]. These different detection and analysis methods have already promoted AUC to a new level that is able to provide a solid strategy for examining a protein's quaternary structural state and conformational changes, as well as various heterogeneous biomolecular interactions [4].

The present study describes our application of AUC to protein size-and-shape distribution analysis and enzyme structure–function analysis. In the first section, the main protease (Mpro) from severe acute respiratory syndrome coronavirus (SARS-CoV) is chosen as an explicit example to illustrate the usefulness of AUC in enzyme research. The AUC method used here is band-sedimentation velocity, also known as active enzyme centrifugation [5,6]. The detailed theoretical background and practical aspects have been thoroughly discussed [7–12]. At that time, the complicated data analysis problems impeded the wide spread use of this technique [9]. The available literature on band-forming AUC is rather scarce. This has changed because advances in software have made handling huge datasets only a few keyboard strokes away [3,4,13,14]. Taking advantage of this, we have successfully applied the active enzyme centrifugation technique to the dimeric SARS-CoV Mpro in which dimerization is required for its normal functioning [15,16]. The enzyme was assayed by band-forming AUC at various concentrations of the substrates. The quaternary structural change and activities of the enzyme during the catalytic process are determined simultaneously. The enzyme velocities are then used in a kinetic model evaluation, which allows the derivation of the kinetic parameters K_m, k_{cat}, and the Hill coefficient for subunit cooperativity. All the results from the AUC support the existence of substrate-induced dimerization of Mpro, which is consistent with our other studies [16].

* Corresponding author. Address: Department of Life Sciences and Institute of Genome Sciences, National Yang-Ming University, 155 Li-Nong Street, Sec. 2, Taipei 112, Taiwan. Fax: +886 2 28202449.
E-mail address: cychou@ym.edu.tw (C.-Y. Chou).

[1] *Abbreviations used:* AEC, active enzyme centrifugation; AUC, analytical ultracentrifugation; SV, sedimentation velocity; pNA, para-nitroanilide; TQ6-pNA, Thr-Ser-Ala-Val-Leu-Gln-para-nitroanilide; SARS-CoV, severe acute respiratory syndrome coronavirus; Mpro, main protease; apoE, apolipoprotein; DHPC, dihexanoylphosphatidylcholine; PBS, phosphate-buffered saline (pH 7.6).

1046-2023/$ - see front matter © 2010 Elsevier Inc. All rights reserved.
doi:10.1016/j.ymeth.2010.11.002

The conformation of proteins after binding a specific ligand is another intriguing issue that has been studied using many other biophysical probes such as nuclear magnetic resonance, surface plasmon resonance, and fluorescence. [17–19]. Most of these methods are not able to investigate delicate structural changes at the quaternary structure level as yet. In the second part of this study, we describe an elaborate application of sedimentation velocity (SV) to the analysis of changes in protein size-and-shape distribution in either an aqueous or lipid environment. The protein chosen for this study was human apolipoprotein E3 (apoE3), a lipid-binding protein found in blood that is responsible for lipid transfer between organs [20]. The sample used in this study was apoE3-(72–166), which is presumed to have an amphipathic α-helical structure [21]. The experiments were executed with and without lipids and then analyzed by $c(s,f_r)$ two dimensional (2d) distribution model [13]. Instead of fitting the anhydrous frictional ratio (f_r) as a fix value, the 2d model is used to set a broad range for f_r during data processing. This modification helps us quantitatively characterize the size-and-shape distribution of apoE3-(72–166) in an aqueous and in a lipid environment.

As a tool that can detect in a few hours both protein quaternary structural/conformational changes in relation to either ligand binding or lipid binding, the power of AUC is not close to being fully explored. AUC can give us not only a qualitative answer, but also a quantitative measurement that is able to explain the interactions between biomolecules and how this relates to their biological functioning.

2. Description of the methods

2.1. Analysis of enzyme structure-and-function relationship in the presence of substrate

Here Mpro was used as an example to illustrate the usefulness of band-forming AUC when elucidating the role of quaternary structural changes in enzyme activity regulation. Mpro is a dimeric protein whose monomer has no catalytic activity [15,22,23]. Our previous studies have suggested that the dimerization can be induced and then further stabilized by substrate binding [16]. However, such structure-and-function investigations have always been performed in separate experiments, and it is never been possible to have identical experimental conditions. Now, by using the band-forming AUC technique, all of these technical problems have been resolved spontaneously and all of the informative data can be captured simultaneously.

A commercially available double-sector Vinograd-type [11] band-forming centerpiece (Beckman, Fullerton, CA, USA) was used for the sedimentation velocity experiments [24]. In the cell, the protein is transferred, on initiation of centrifugation, through a small channel from the sample well to the bulk sector space, which contains a substrate solution of greater density than the protein solution. The proteins will migrate as a narrow band during the sedimentation run and this created the technique's name, band-forming centrifugation. Moreover, in the presence of ligands, concentration changes in the ligands can be detected using a usual AUC detector, if the substrate-product reaction cycle involves a spectrometric or fluorometric change. This allows the measurement of enzyme function by an *in situ* kinetic assay.

2.1.1. Sample preparation

In our experiment, SARS-CoV Mpro with a 6×His tag fusion was expressed in *Escherichia coli* and purified by nickel affinity chromatography [15]. After a buffer changed using an Amicon 10K cutoff filter (Millipore, Bedford, MA, USA), the protein was stored in PBS (pH 7.3) at 4 °C. The substrate used for the assay was a synthetic hexapeptide derivative, Thr–Ser–Ala–Val–Leu–Gln–para-nitroanilide (TQ6-pNA) (purity 95–99% by HPLC), which was obtained from GL Biochem Ltd., Shanghai, China [16,25]. The enzymatic activity of Mpro was measured by a colorimetric-based peptide cleavage assay. Any increase in absorbance at 405 nm caused by para-nitroanilide (pNA) releasing was continuously monitored using a spectrophotometer. The amount of pNA released from the proteolysis is calculated using a standard curve generated by analytical grade pNA and the result is consistent with the literature ($A_{405\ nm}$ = 9.8 at 1 mM) [26].

To get a narrow protein band, the bulk substrate solution has to be denser than the protein solution. Usually, D_2O, glycerol, sucrose, or high salt (e.g., 50–100 mM excess) is chosen for this purpose [27]. We use D_2O because highly purified D_2O is commercially available; in addition, the handling of a viscous liquid is avoided, which greatly reduces the experimental lapsed time. Each sedimentation run in D_2O is completed within a couple hours rather than overnight, which is required if glycerol is used.

2.1.2. Band-forming sedimentation velocity

The AUC experiments are performed on a XL-A analytical ultracentrifuge (Beckman, Fullerton, CA, USA) with an An-50 Ti rotor [20]. In the sample well of the double-sector band-forming centerpiece, 15 μl of Mpro (1 mg/ml) was added before the cell was assembled. The other small well above the reference sector can be left empty. In total, 330 μl of substrate at different concentrations was dissolved in D_2O and then loaded into the bulk sample sector space. After equilibrating to the desired temperature, the centrifugation was spun at a rotor speed of 42,000 rpm. We found that the TQ6-pNA was cleaved and free pNA accumulated during centrifugation (detected by absorbance change at 405 nm). The absorbance spectrum of the free pNA interferes with protein absorbance at 280 nm. Therefore absorbance at 250 nm was chosen instead for detecting the protein band, while the wavelength 405 nm was used to monitor the catalytic released product pNA. The spectrum was monitored continuously using a time interval of 600 s per scan and a step size of 0.003 cm.

A typical trace of the 250 nm and 405 nm spectral results are shown in Figs. 1A and 2A, respectively. The dataset from these multiple scans at 250 nm at different time intervals were then fitted to a continuous $c(s)$ distribution model using the SEDFIT program [4,13] (<www.analyticalultracentrifugation.com>) (cited August 1, 2010). The partial-specific volume of Mpro, the solvent density, and the viscosity were calculated by SEDNTERP (<www.jphilo.mailway.com/download.htm>) (cited August 1, 2010). The first six scans at 405 nm were used to calculate the integration area in order to derive the initial velocity values.

2.1.3. Data analysis

2.1.3.1. Continuous c(s) distribution analysis for band-sedimentation velocity. SEDFIT calculates the continuous size distribution (sedimentation coefficient) using a variation based on the Lamm equation [28]. The observed continuous $c(s)$ distribution profiles can be treated as a superimposition of each subpopulation $c(s)$ of particles with sedimentation coefficients between s and $s + ds$ using the following equation,

$$a(r,t) \cong \int c(s)L(s,D(s),r,t)ds + \in \quad (1)$$

where $a(r,t)$ represents the experimentally observed signal at radius r and time t. $L(s, D(s), r, t)$ is the sedimentation profile of an ideally sedimenting monodisperse species with sedimentation coefficient s and diffusion constant D, and were calculated as the solution to the Lamm equation; $\in$ represents the noise components. In the data fitting process, the Tikhonov–Phillips method is implemented by SEDFIT [4,29] and is used at default to regularize the distribution. All

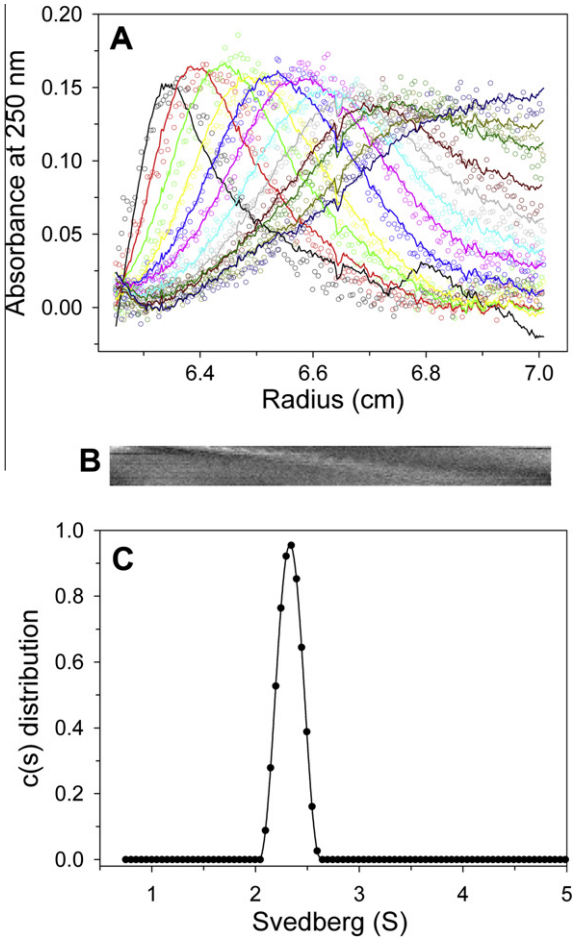

Fig. 1. Band-forming active enzyme centrifugation of Mpro in the presence of 200 μM substrate. (A) A typical trace of absorbance at 250 nm of the enzyme during the experiment. The symbols are experimental data and the lines are the results fitted to the Lamm equation using the SEDFIT program. (B) The residual bitmap of the raw data and the best-fit results. (C) Continuous $c(s)$ distribution from the best fit analysis. The species at $S = 2.3$ corresponds to the dimeric Mpro. The protein amount used is 15 μl (1 mg/ml) in PBS (pH 7.6). The substrate at 200 μM was dissolved in D_2O to give a higher density, which sharpens the protein band when the centrifugation begins. Total volume is 330 μl.

continuous size distributions are calculated using a confidence level of $p = 0.99$, a best fitted average of f_r, a resolution value N of 200, and for sedimentation coefficients between 0.1 and 15.0 S.

In Fig. 1A, the lines show the results of best-fitting to the $c(s)$ distribution. The residuals bitmap displays the quality of the fit (Fig. 1B). This maps the residual values to a pixel brightness value that is linearly scaled between −0.04 and 0.04 from black to white. For perfect residuals, this will result in a homogeneous picture. A typical best-fit size distribution plot is shown in Fig. 1C. In the presence of 200 μM substrate, Mpro exists as a single species at $S = 2.3$, which corresponds to the dimeric form [16].

2.1.3.2. Initial velocity and enzyme kinetic parameters calculation. In our study, during the process of centrifugation, each cell is measured sequentially by an absorbance of 250 nm and then of 405 nm. At a rotor speed of 42,000 rpm, each scan takes about 1 min; thus there is a requirement for 10 min intervals between successive scans at 405 nm if five sample cells are used (Fig. 2A). In the catalytic initial velocity (v_0) calculation, we integrate the area of the first five spectra (scan 2–6) to estimate the product-release rate. Next, the progress curves for a set of enzyme-catalyzed reactions with different concentrations of substrate can be plotted (Fig. 2B). The initial velocities of the enzyme are obtained from

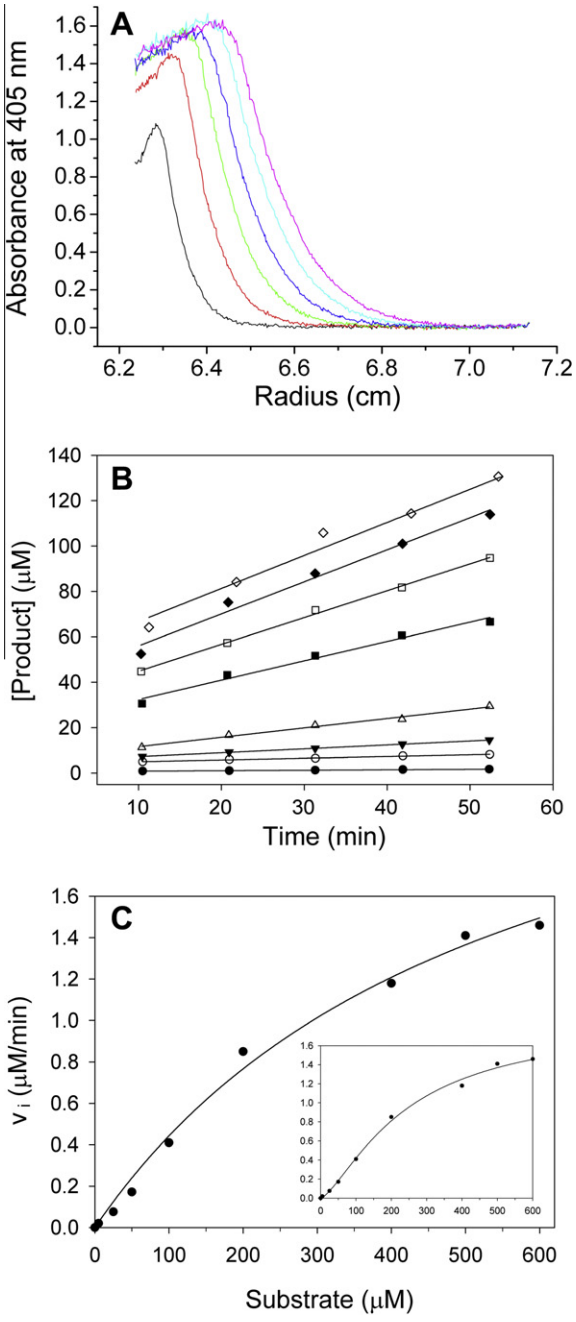

Fig. 2. Monitoring of enzymatic activity of Mpro during band-forming ultracentrifugation. The same cell in Fig. 1 was followed using the enzymatic reaction under identical conditions as described above. Panel (A) shows the absorbance at 405 nm trace for the released product (pNA) after the first hour of the experiment. The time interval of each spectrum from black to pink color is 10 min. Panel (B) showed the product at different time with different substrate concentrations (close circle: 5 μM; open circle: 25 μM; close triangle, 50 μM; open triangle, 100 μM; close square, 200 μM; open square, 400 μM; close diamond, 500 μM; and open diamond, 600 μM). The lines indicated the best-fit results for initial velocity calculation. Panel (C) showed the plot of initial velocities versus substrate concentrations. The line represented best-fit results according to the Michaelis–Menten equation. The inset plot shows the same data fitted to the Hill equation. The kinetic parameters derived are shown in Table 1.

the slopes of the lines. Next, the steady-state enzyme kinetic parameters were obtained by fitting the initial velocity data to the Michaelis–Menten Eq. (2).

$$v_0 = k_{cat}[E][S]/(K_m + [S]) \quad (2)$$

where k_{cat} is the catalytic constant, [E] is the enzyme concentration, [S] is the substrate concentration, and K_m is the Michaelis constant for the substrate. The same data were also examined for any possible cooperativity effect. Then the kinetic parameters are derived by fitting the initial velocity data to the Hill Eq. (3)

$$v_0 = k_{cat}[E][S]^h/(K' + [S]^h) \quad (3)$$

where K' is a constant that relates to the dissociation constant and h is the Hill coefficient. The program SigmaPlot (Systat Software Inc., Richmond, CA, USA) was used for the data analysis. Fig. 2C shows a typical saturation curve and the best-fit kinetic parameters are shown in Table 1. The inset in Fig. 2C shows the results fitted by Hill equation best.

2.1.4. Data interpretation

For the first time, the quaternary structure and the enzyme activity of SARS–CoV Mpro could be determined simultaneously under identical conditions. Based on the $c(s)$ distribution analysis, we observe that there are quaternary structural changes at various substrate concentrations (Fig. 3). This is consistent with our recent observations during routine SV experiments, which have shown that the presence of substrate can induce a quaternary structural change in Mpro [16]. A broad peak located between the monomeric and dimeric Mpro was detected at a substrate concentration of 50 μM, which suggest that Mpro is a rapidly self-associating protein [16]. Moreover, all Mpro molecules associate into a dimeric form when the substrate concentration is over 100 μM.

The enzyme catalytic activities at the various substrate concentrations were obtained concurrently. This enzyme kinetic dataset was further analyzed by fitting the results to the Michaelis–Menten and Hill equations (Fig. 2C and inset). We found that the data gave a better fit with the Hill equation, where R_{sqr} = 0.997, while the fit of the Michaelis–Menten equation was 0.994 (Table 1). The Hill coefficient of 1.4 suggests that there seems to be positive cooperativity between the two subunits of the dimeric Mpro [16]. According to the $c(s)$ distribution (Fig. 3), the sigmoidal trend at low [s] is due to the lower dimer content. The substrate-induced dimerization and activation of Mpro that has been observed previously using steady-state enzyme kinetics is confirmed and now should be considered real.

2.2. Analysis of protein size-and-shape distribution in various lipid environments

In the second part of this study, we used another system that demonstrates the application of AUC to the analysis of protein size-and-shape distribution, this time in various lipid environments. There are many proteins, such as apolipoproteins or membrane proteins, the quaternary structure of which in aqueous environment is very different to that found in a lipid environment [20,30]. Apolipoproteins are lipid-transferring proteins. Binding of a lipid molecule to the protein induces a conformational change in the macromolecule that is closely correlated to its intrinsic biological function. What is required is a reliable quantitative method for measuring this conformation change. Using SV experiments and a new powerful distribution model implemented in SEDFIT (see below), we can precisely analyze these intricate structural changes with confidence. The protocol described below illustrates how this approach allows one to study this issue.

Table 1
Enzyme kinetic parameters of Mpro produced by fitting to the two different models.

Model	K_m (μM)	k_{cat} (s^{-1})	k_{cat}/K_m ($s^{-1}M^{-1}$)	R_{sqr}
Michaelis–Menten	543.6 ± 114.4	0.04 ± 0.005	74 ± 18	0.9936
	K′ (10^3 μM)	k_{cat} (s^{-1})	h	
Hill cooperative	2.2 ± 1.4	0.02 ± 0.002	1.40 ± 0.16	0.9972

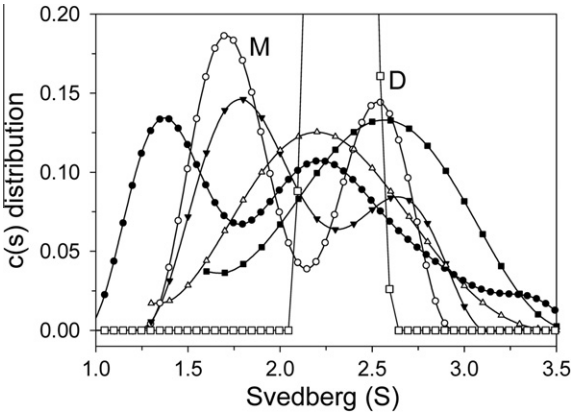

Fig. 3. Effects of substrate concentration on the quaternary structure of Mpro measured by band-forming ultracentrifugation. Different curves represented the continuous c(s) distribution of Mpro at substrate concentration of 0 (filled circle), 5 (open circle), 25 (filled triangle), 50 (open triangle), 100 (filled square), and 200 (open square) μM. The labels M and D showed the position of the monomer and dimer species, respectively. To clearly display the other results, that for 200 μM (Fig. 2C showed the full scale) is only partially shown. According to our previous studies, the result at 50 μM substrate, which showed a broad peak between monomer and dimer, suggested that Mpro is a rapid self-association protein.

2.2.1. Sample preparation

The protein sample preparation is the same as that described in Section 2.1.1 and the details are described in Ref. [17]. Human apoE3-(72–166) protein is used in this study as an example. This protein has an amphipathic α-helical structure that can bind to lipid particles very efficiently (Chou et al., unpublished data). In the present study, the lipid molecule used was dihexanoylphosphatidylcholine (DHPC). DHPC has a critical micelle concentration of 16 mM at which the micelle monomers formed contain 40 molecules, based on light scattering and ultracentrifugation data [31]. Here we use two concentrations of DHPC (5 and 50 mM) to establish an appropriate lipid environment that contains either DHPC submicelles or micelles, respectively. Before executing the AUC experiments, protein at a suitable concentration (0.5 mg/ml) and DHPC solution are mixed and incubated at 4 °C for 16-h to stabilize the system.

2.2.2. Sedimentation velocity

The SV experiments were performed using an XL-A analytical ultracentrifuge with a standard 12-mm double-sector *epon* charcoal-filled centerpieces (Beckman, Fullerton, CA, USA) [17,20]. Initially, the samples (380 μl protein solution) and reference (400 μl solvent only) are loaded into the cell and mounted in an An-50 Ti rotor. Three sample solutions, with apoE3-(72–166) protein preincubated in PBS, PBS + 5 mM, or PBS + 50 mM DHPC were loaded into different cells. After balancing and putting a counterbalance into the last rotor chamber, the experiments were started at a rotor speed of 3000 rpm as a pre-scan check for sample leakage. When the vacuum was lower than 50 μ and the temperature was stable at 20 °C, the rotor speed was increased to 42,000 rpm and the absorbance at 280 nm monitored in a continuous mode at time intervals of 480 s and a step size of 0.003 cm. A typical run takes 4–6-h.

Fig. 4 shows the raw SV results for apoE3-(72–166) protein in the presence of 0, 5, and 50 mM DHPC. At the different DHPC concentration, the signal profiles of the same protein are significantly different. The multiple scans obtained at different time intervals were then analyzed by the SEDFIT program [4,32].

2.2.3. $c(s,f_r)$ 2d distribution analysis

SEDFIT program is a powerful software program for analyzing the size distribution using SV raw data [4,32]. The present version (after version 9.2f) has implemented a new approach in order to evaluate macromolecular size-and-shape distributions and this is called $c(s,f_r)$ 2d distribution [13]. Such a distribution can be conveniently calculated as the equivalent size-and-shape distributions of sedimentation coefficients, and can be transformed to the other parameters as well, such as Stokes radii (R_s), molar masses, and diffusion coefficients.

In our study, the 2d distributions are solved and regularized at a confidence level of $p = 0.95$ by maximum entropy, and a resolution of 200 for sedimentation coefficients between 0.1 and 20 *S*. The f_r was an equidistant grid from 1.0 to 3.5 with 0.25 steps. The detailed theories underlying these analyses have been described previously by Brown and Schuck [13]. Briefly, a differential distribution of sedimentation coefficients and frictional ratios $c(s,f_r)$ can be defined as

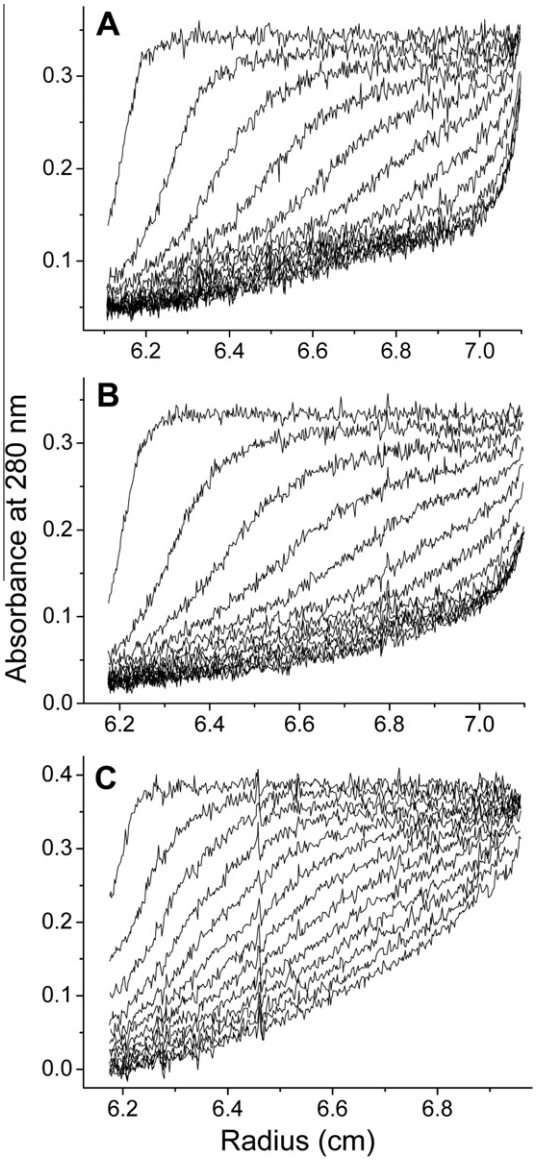

Fig. 4. Representative SV raw data subset of apoE3-(72–166) protein. The experiments were run at a rotor speed of 42,000 rpm at 20 °C. Traces were calculated at time intervals of 480 s. For clarity, only every sixth scan is shown. The A–C indicated the results of apoE3-(72–166) protein in PBS (pH 7.3) (aqueous), or 5 mM, and 50 mM DHPC (lipid) solutions, respectively.

$$a(r,t) = \int\int c(s,f_r)\chi(s,D(s,f_r),r,t)\,ds\,df_r \tag{4}$$

with $a(r,t)$ denoting the total signal as a function of distance from the center of rotation, r, and time, t, with $\chi(s,D,r,t)$ denoting the solution of the Lamm equation [28]

$$\frac{\partial\chi}{\partial t} = \frac{1}{r}\frac{\partial}{\partial r}\left[rD\frac{\partial\chi}{\partial r} - s\omega^2 r^2\chi\right] \tag{5}$$

in which $D(s,f_r)$ denotes the dependence of the diffusion coefficient on the sedimentation coefficient and frictional ratio, given as

$$D(s,f_r) = \frac{\sqrt{2}}{18\pi}kTs^{-1/2}(\eta f_r)^{-3/2}((1-\overline{v}\rho)/\overline{v})^{1/2} \tag{6}$$

(containing the Boltzmann constant k, absolute temperature T, macromolecular partial-specific volume $\overline{v}$, solvent viscosity η, and solvent density ρ) [4].

2.2.4. Data analysis and interpretation

Fig. 5 shows the results of best fitting of our data to the $c(s,f_r)$ 2d distribution. The inset figures are the residual bitmaps that indicate the quality of each data fitting. These map the residual values to a pixel brightness value that is linearly scaled between −0.02 and 0.02 from black to white. From the analysis, we can compare the size-and-shape distribution (colored mesh peaks) of a protein in aqueous or the various lipid environments (Fig. 5A–C). Below the $c(s,f_r)$ surface is shown a contour plot of the distribution projected onto the s–f_r plane, where the magnitude of $c(s,f_r)$ is indicated by contour lines at constant $c(s,f_r)$ at equidistant intervals. Our studies on apoE3-(72–166) protein suggested that the large protein species found in PBS or in 5 mM DHPC solution dissociates into a smaller protein species in 50 mM DHPC solution (Fig. 5A and B vs. 5C).

Furthermore, SEDFIT also provides a function that allows the calculation of the integration of a species or over a range. This gives precise sedimentation coefficients, molar masses, and R_s for quantitative comparisons (Table 2). After calculating the content of the distribution, it was found that there was a 30% monomer–dimer mixture ($S = 1.8$, mass = 16.2 kDa, and $R_s = 1.9$ nm) in PBS (Fig. 5A). The same species ($S = 1.9$, mass = 37.5 kDa, and $R_s = 4.4$ nm) was found to be maintained in a more extended shape ($f_r > 2$) in the submicellar solution (Fig. 5B). At this stage, this will increase the protein's hydrophobic exposure such that protein polymerization is induced. That is why this species decreases and other larger species increase. This suggested that apoE3-(72–166) begins to maintain a looser, and more extended conformation in a submicellar environment. In 50 mM DHPC, 93% of the apoE3-(72–166) protein is dissociated to form an elongated monomer that has a smaller S value (1.0) and a larger R_s value (3.0 nm) (Fig. 5C). Furthermore, the f_r contour of the apoE3-(72–166) monomer species in a 50 mM DHPC micellar solution shows a wider distribution compared to PBS. From these observations, we were able to derive a quantitative way of evaluating the size-and-shape distribution changes of a protein as it moves from an aqueous to a lipid environment.

3. Application and limitations

AUC was invented by Svedberg in 1923 [33] (Nobel Laureate, Chemistry, 1926). The system becomes a practical tool for the analysis of bipolymer heterogeneity when UV/VIS absorption optics and Rayleigh interference optics were developed. The rebirth of modern AUC started in the 1990s when the acquisition and management of huge amount of data became feasible. Almost at the same time, some powerful programs such as SVEDBERG (<www.jphilo.mailway.com/svedberg.htm>) (cited August 1,

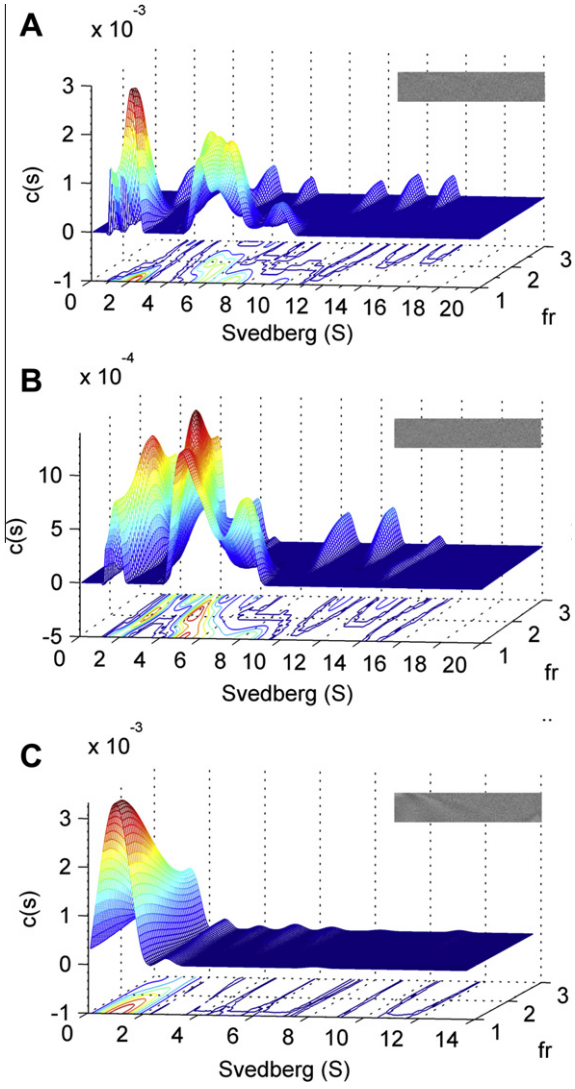

Fig. 5. Continuous $c(s,f_r)$ 2d distribution analysis of apoE3-(72–166) protein in aqueous or lipid environments. (A–C) apoE3-(72–166) in PBS, 5 mM, and 50 mM DHPC, respectively. The protein concentration was 0.5 mg/ml. The *x*, *y*, and *z* axes show the sedimentation coefficients (S), local concentration $c(s)$, and anhydrous frictional ratio (f_r), respectively. The colors define the local concentration of the species (red to blue: high to low). Contour plots are shown at the bottom. Insets, a grayscale of the residual bit map showing the data fitting quality. Calculation based on the SEDFIT program.

2010), ULTRASCAN (<www.cauma.uthscsa.edu>) (cited August 1, 2010), SEDFIT, SEDPHAT (<www.analyticalultracentrifugation.com/sedphat>) (cited August 1, 2010), and SEDANAL (<http://rasmb.bbri.org/software/windows/sedanal-stafford/>) (cited August 1, 2010) were also launched. Although AUC data analysis has reached a mature stage with comprehensive mathematics, some of the above-mentioned programs are still being updated by the developers every few months. Each update gives us more selections when analyzing AUC data. These advances in both instrumentation and software analysis have allowed AUC to be used to study more complicated structural change including those during the binding of ligands to the proteins. In our example, the dimerization of Mpro is induced by substrate binding and was detected by band-forming active enzyme centrifugation. The enzymatic reaction is followed by observing the absorbance change at 405 nm versus time. The kinetic data obtained suggest that the subunits of the wild-type dimer are cooperative during the catalytic cycle, which cannot be detected in some routine kinetic assays using a typical spectrometry or fluorescence instrument; nonetheless, this process can be clearly demonstrated in some Mpro mutants [16]. Thus using AEC on Mpro, it was possible to differentiate and identify the cooperativity that traditional enzyme kinetic assay might have missed.

However, the AEC technique that was employed in this study has some limitations. First of all, the enzymatic reaction usually has high efficiency. This means that very small amount of enzyme is sufficient to catalyze a reaction that can be detectable using a routine spectrophotometer, spectrofluorometer or other means. The protein peak usually is invisible under these assay conditions. There have been many successful applications of AEC in literature [5,6,8,34–41]. In most cases, the sedimentation coefficients are derived from the release of the product, which is presumed to be produced by the catalytically active site and thus indicates the position of the active enzyme–substrate complex. Mpro is an ideal model system to demonstrate the usefulness of AEC using an *in situ* protein band system via direct determination as we noticed before [42]. The enzyme is a simple monomer–dimer system. The enzymatic reaction rate is moderate, and a large amount of protein is required for catalysis. In our case, the absorbance of the ligand and protein partially overlapped, the protein signal was severely interfered with by the high concentration of substrate. This resulted in a high level of system noise when the data is analyzed (Fig. 1B). When the concentration of substrate is over 200 μM, the size distribution of the protein cannot be analyzed precisely. To circumvent this, the protein may be labeled with fluorescein [43], which allows the protein fluorescence signal be detected at 494 nm. This may be able to separate the signal from the protein from that of the ligand. A fluorescence detector for AUC is good hardware to acquire in order to solving this problem, although the detector is expensive. (<www.avivbiomedical.com/aufds.php>) (cited April 29, 2010).

Table. 2
Continuous $c(s,f_r)$ 2d distribution of apoE3-(72–166) protein in PBS or lipid environments.

ApoE3-(72–166) in	Integral range (S)	S_w (S)	Mass (kDa)	R_s (nm)	Integral area
PBS	0.7–3.2	1.8 ± 0.4	16.2 ± 6.4	1.9 ± 0.5	0.090 (30%)
	3.2–4.4	4.0 ± 0.2	137.1 ± 42.3	7.6 ± 2.2	0.040 (13%)
	4.4–6.1	5.1 ± 0.4	112.5 ± 47.1	5.0 ± 2.3	0.118 (39%)
	6.2–7.5	6.8 ± 0.4	136.8 ± 81.4	4.5 ± 2.8	0.022 (7%)
	7.5–16.5	–	–	–	0.032 (11%)
5 mM DHPC	1.2–2.5	1.9 ± 0.2	37.5 ± 17.4	4.4 ± 2.0	0.053 (19%)
	3.3–4.4	4.0 ± 0.3	139.6 ± 38.6	7.9 ± 2.2	0.057 (20%)
	4.4–5.5	4.9 ± 0.3	119.6 ± 53.1	5.5 ± 2.5	0.067 (24%)
	5.5–7.0	6.0 ± 0.4	150.0 ± 92.1	5.6 ± 3.5	0.039 (14%)
	7.0–9.5	8.0 ± 0.5	153.5 ± 41.5	4.3 ± 1.1	0.028 (10%)
	9.5–16.5	–	–	–	0.037 (13%)
50 mM DHPC	0.2–2.1	1.0 ± 0.4	17.7 ± 14.7	3.0 ± 1.7	0.376 (93%)
	2.2–3.3	2.7 ± 0.2	84.0 ± 35.6	6.0 ± 2.6	0.013 (3%)
	3.3–12.5	–	–	–	0.016 (4%)

Another limitation is the detection time. At a rotor speed of 42,000 rpm, each absorbance scan takes about 1 min. This is too long and enzyme activity might be underestimated for some highly active enzymes. It may be possible to circumvent this problem using an alternate substrate with a lower efficiency or a mutant enzyme with a lower enzymatic activity. Recently, a multiwavelength UV/VIS detection for AUC has been developed and successfully applied to investigating β-carotene–gelatin composite particles [2]. It can shorten the detection time by measuring several wavelengths simultaneously.

In this article, we use SEDFIT for our data analysis. There is no limitation to how you handle AUC data and many other superb software programs are available [44–46]. New versions of SEDFIT and other software will allows other interesting areas to be explored in the future.

4. Concluding remarks

Here we have introduced some applications of AUC and explored protein size-and-shape distribution analysis and structure-and-function analysis in the presence of ligands. Band-forming sedimentation velocity can follow quaternary structural changes of an active enzyme as the ligand is bound. The enzyme kinetic parameters thus obtained are comparable to those from routine enzyme kinetic assays, and may be more informative. The results of sedimentation velocity studies can be further explored by $c(s,f_r)$ 2d distribution analysis, which provides information about the protein size-and-shape changes. Up to this moment, no other biophysical or biochemical methods can surpass AUC, which can be used over a few hours to examine protein quaternary structure or protein conformational changes. AUC can provide not only qualitative information, but also quantitative measurements that go a long way in explaining the interactions between biomolecules and their biological functions. The rapid progress of AUC in recent years, both hardware and software, has resulted in a situation, we strongly feel, where the powerfulness of AUC is somehow underestimated. With a wider use of AUC, especially when complemented with other delicate biophysical instruments, the datasets originating from AUC analysis of complicated biological phenomena will become manageable.

Acknowledgments

This study was supported by grants from National Health Research Institute, Taiwan (NHRI-EX99-9947SI) and National Science Council, Taiwan (98-2320-B-010-026-MY3) to C.Y.C.

References

[1] E. Karabudak, Development of MWL-AUC/CCD-C-AUC/SLS-AUC detectors for the analytical ultracentrifuge, Ph.D. Dissertation, Max Planck institute of colloids and interfaces, Potsdam, Germany, 2009, pp. 1–115.
[2] E. Karabudak, W. Wohlleben, H. Colfen, Eur. Biophys. J. 39 (2010) 397–403.
[3] D.J. Scott, S.E. Harding, A.J. Rowe (Eds.), Modern Analytical Ultracentrifugation: Techniques and Methods, Royal Society of Chemistry, UK, 2005.
[4] P. Schuck, Biophys. J. 78 (2000) 1606–1619.
[5] R. Cohen, M. Mire, Eur. J. Biochem. 23 (1971) 267–275.
[6] D.J. Llewellyn, G.D. Smith, Arch. Biochem. Biophys. 190 (1978) 483–494.
[7] J.M. Claverie, H. Dreux, R. Cohen, Biopolymers 14 (1975) 1685–1700.
[8] R. Cohen, M. Mire, Eur. J. Biochem. 23 (1971) 276–281.
[9] R. Cohen, J.M. Claverie, Biopolymers 14 (1975) 1701–1716.
[10] D.L. Kemper, J. Everse, Methods Enzymol. 27 (1973) 67–82.
[11] J. Vinograd, R. Bruner, R. Kent, J. Weigle, Proc. Natl. Acad. Sci. USA 49 (1963) 902–910.
[12] J. Vinograd, R. Radloff, R. Bruner, Biopolymers 3 (1965) 481–489.
[13] P.H. Brown, P. Schuck, Biophys. J. 90 (2006) 4651–4661.
[14] P. Schuck, Anal. Biochem. 320 (2003) 104–124.
[15] C.Y. Chou, H.C. Chang, W.C. Hsu, T.Z. Lin, C.H. Lin, G.G. Chang, Biochemistry 43 (2004) 14958–14970.
[16] S.C. Cheng, G.G. Chang, C.Y. Chou, Biophys. J. 98 (2010) 1327–1336.
[17] C.Y. Chou, W.P. Jen, Y.H. Hsieh, M.S. Shiao, G.G. Chang, J. Biol. Chem. 281 (2006) 13333–13344.
[18] C.S. Gangabadage, J. Zdunek, M. Tessari, S. Nilsson, G. Olivecrona, S.S. Wijmenga, J. Biol. Chem. 283 (2008) 17416–17427.
[19] M.D. Griffin, M.L. Mok, L.M. Wilson, C.L. Pham, L.J. Waddington, M.A. Perugini, G.J. Howlett, J. Mol. Biol. 375 (2008) 240–256.
[20] C.Y. Chou, Y.L. Lin, Y.C. Huang, S.Y. Sheu, T.H. Lin, H.J. Tsay, G.G. Chang, M.S. Shiao, Biophys. J. 88 (2005) 455–466.
[21] Y.H. Hsieh, C.Y. Chou, unpublished data.
[22] W.C. Hsu, H.C. Chang, C.Y. Chou, P.J. Tsai, P.I. Lin, G.G. Chang, J. Biol. Chem. 280 (2005) 22741–22748.
[23] P.Y. Lin, C.Y. Chou, H.C. Chang, W.C. Hsu, G.G. Chang, Arch. Biochem. Biophys. 472 (2008) 34–42.
[24] J. Lebowitz, S. Kar, E. Braswell, S. McPherson, D.L. Richard, Protein Sci. 3 (1994) 1374–1382.
[25] C. Huang, P. Wei, K. Fan, Y. Liu, L. Lai, Biochemistry 43 (2004) 4568–4574.
[26] N. Strater, L. Sun, E.R. Kantrowitz, W.N. Lipscomb, Proc. Natl. Acad. Sci. USA 96 (1999) 11151–11155.
[27] S.E. Harding, A.J. Rowe, in: P.C. Engel (Ed.), Enzymol. LabFax, Bios Scientific, Oxford, 1996, pp. 66–75.
[28] O. Lamm, Ark. Mat. Astr. Fys. 21B (1929) 1–4.
[29] D.L. Phillips, J. Assoc. Comput./Mach. 9 (1962) 84–97.
[30] M.A. Perugini, P. Schuck, G.J. Howlett, J. Biol. Chem. 275 (2000) 36758–36765.
[31] R.J. Tausk, J. Karmiggelt, C. Oudshoorn, J.T. Overbeek, Biophys. Chem. 1 (1974) 175–183.
[32] P. Schuck, M.A. Perugini, N.R. Gonzales, G.J. Howlett, D. Schubert, Biophys. J. 82 (2002) 1096–1111.
[33] T. Svedberg, J.B. Nichols, J. Amer. Chem. Soc. 45 (1923) 2910–2917.
[34] C.H. Emes, A.J. Rowe, Biochim. Biophys. Acta 537 (1978) 125–144.
[35] U. Hommel, A. Lustig, K. Kirschner, Eur. J. Biochem. 180 (1989) 33–40.
[36] C.S. Johnson, W.C. Deal Jr., J. Biol. Chem. 257 (1982) 913–916.
[37] D.W. Martin, Biochemistry 22 (1983) 2276–2282.
[38] A. Modrak-Wojcik, K. Stepniak, V. Akoev, M. Zolkiewski, A. Bzowska, Protein Sci. 15 (2006) 1794–1800.
[39] A. Pasquo, K.L. Britton, T.J. Stillman, D.W. Rice, H. Colfen, S.E. Harding, R. Scandurra, P.C. Engel, Biochim. Biophys. Acta 1297 (1996) 149–158.
[40] J.M. Pionetti, Biochem. Biophys. Res. Commun. 58 (1974) 495–498.
[41] S.L. Snyder, I. Wilson, W. Bauer, Biochim. Biophys. Acta 258 (1972) 178–187.
[42] G.G. Chang, in: S.K. Lal (Ed.), Molecular Biology of the SARS–Coronavirus, Springer-Verlag, Berlin Heidelberg, 2010, pp. 115–128.
[43] N. Sanchez-Puig, D.B. Veprintsev, A.R. Fersht, Protein Sci. 14 (2005) 1410–1418.
[44] B. Demeler, in: D.J. Scott, S.E. Harding, A.J. Rowe (Eds.), Modern Analytical Ultracentrifugation: Techniques and Methods, Royal Society of Chemistry, UK, 2005, pp. 210–229.
[45] J.S. Philo, Biophys. J. 72 (1997) 435–444.
[46] W.F. Stafford, Methods Enzymol. 323 (2000) 302–325.